Kinetics of the ClO + HO_2 reaction over the temperature range T = 210 – 298 K

Michael K.M. Ward[†] and David M. Rowley*

*Department of Chemistry, UCL, 20 Gordon Street, London WC1H 0AJ, UK.
[†] Laboratoire PC2A/CNRS, Université de Lille 1, 59655, Villeneuve d'Ascq, France

Abstract

The rate coefficient for the atmospherically important radical reaction:

$$ClO + HO_2 \rightarrow \text{Products} \qquad (1)$$

which leads to ozone depletion, has been studied over the temperature range T = 210 – 298 K and at ambient pressure p = 760 ± 20 Torr. The reaction was studied using laser flash photolysis radical generation coupled with broadband charge coupled device absorption spectroscopy employing a two-dimensional charge-coupled-device (CCD) detection system. ClO radicals were generated following the photolysis of Cl_2 and Cl_2O gas mixtures diluted in nitrogen and oxygen. ClO radicals were monitored using broadband fingerprinting of their characteristic vibronic ($A^2\Pi \leftarrow X^2\Pi$) spectral structure, representing a definitive monitoring of this radical. Addition of hydroperoxy radical precursors to the gas mixture (methanol and oxygen) subsequently led to a competition for photolytically generated Cl atoms and a simultaneous prompt formation of both ClO and HO_2 radicals. Detailed analysis and modelling of the radical production routes provided a degree of constraint into numerical integration simulations which were then used to interrogate and fit to ClO temporal profiles to extract the rate coefficient k_1. The ambient temperature (T = 298 K) rate coefficient reported is $k_1 = (8.5 \pm 1.5)\times10^{-12}$ cm^3 molecule^{-1} s^{-1}. The rate coefficient, k_1, is described by the Arrhenius expression:

$$k_1 = \left(1.74\ ^{+1.56}_{-0.83}\right)\times10^{-12}\exp\left(\frac{474 \pm 161}{T/\mathrm{K}}\right) \text{cm}^3\,\text{molecule}^{-1}\,\text{s}^{-1}$$

where errors are 1σ statistical only. This significant rate coefficient is greater than previously reported, with a stronger negative temperature dependence than previously observed. Consequently this suggests that the contribution of reaction (1) to ozone loss, in particular at mid-latitudes might be currently underestimated in models. This work reports atmospheric pressure kinetic parameters for this reaction which are greater than those reported from low pressure studies, perhaps supporting ClO and HO_2 association as predicted by previous theoretical studies of this process and highlighting the need for further pressure dependent experimental studies of the title reaction, which has been demonstrated here to be effective as an ozone loss process over a wide temperature range.

1. Introduction

Stratospheric ozone loss has been reported for several decades and is of environmental concern, directly affecting the solar UV exposure of all ecosystems.[1] First observed by Farman *et al.,*[2] the near total loss of stratospheric ozone over Antarctica in Spring has since been observed annually, with comparable Springtime ozone loss also being recently observed over the Arctic.[3-5] Following intense investigation, from field campaigns, models and laboratory studies, this issue has become an exemplar of how knowledge of atmospheric processes can in principle mitigate environmental degradation effected by anthropogenic activity. It is now known, for example, that the principal origin of these annual ozone depletion events lies within chlorine chemistry with an anthropogenic source.[1] Solar photolytic degradation of manmade chloroflurocarbons (CFCs) within the stratosphere initiates radical chain chemistry that catalytically destroys ozone. Inorganic chlorine species, specifically Cl and ClO, partake in efficient ozone destroying cycles which are exacerbated by the meteorological conditions predominant in the Polar Wintertime. One such cycle, as was first proposed by Molina and Molina[6] involves the formation and subsequent photolysis of the ClO dimer, Cl_2O_2:

$CFCs + h\nu$	$\rightarrow$	$Cl + O_3$	$\rightarrow$	$ClO + O_2$
$ClO + ClO + M$	$\rightleftharpoons$	$Cl_2O_2 + M$		(2, −2)
$Cl_2O_2 + h\nu$	$\rightarrow$	$ClOO + Cl$		(3)
$ClOO + M$	$\rightarrow$	$Cl + O_2 + M$		(4)
$2(Cl + O_3$	$\rightarrow$	$ClO + O_2)$		(5)
Net: $2O_3 + h\nu$	$\rightarrow$	$3\ O_2$		

This 'ClO dimer' cycle is particularly efficient when ClO abundances are elevated, since the forward reaction (2) may become rate-limiting with a rate proportional to $[ClO]^2$.[7] This situation, which arises in the Polar Springtime, and the extent of the subsequent ozone loss results directly from the preceding chemical transformation of relatively inactive chlorine-containing species into more photolabile species, during the Polar Wintertime, driven by heterogeneous processes through interaction with Polar stratospheric clouds (PSC's).[8,9]

Such processes serve to partition $ClONO_2$ and HCl into the more photolabile species HOCl and Cl_2 which therefore build up in concentration during the Wintertime absence of solar illumination. Upon the return of solar illumination in Spring, these species are then rapidly photolysed and the ensuing formation of enhanced atomic chlorine abundances results in reaction (5) forming elevated ClO abundances and the ClO dimer cycle being the most effective Polar ozone destroying pathway.

By contrast, at mid-latitudes and in the tropics, where the diurnal oscillation of solar irradiation between day and night is more regular throughout the year compared to the Poles, stratospheric ozone destruction through chlorine chemistry is much less pronounced. This is because the accumulation of HOCl and Cl_2 through *heterogeneous* processes is inhibited in the absence of PSC's and so ClO concentrations remain relatively low. However, ozone loss is observed in middle-latitude regions predominantly near the tropopause, spanning the upper troposphere (UT) and lower stratosphere (LS).

Ozone, both a strong ultraviolet (UV) and infrared (IR) absorber, plays a significant role as a filter of solar UV radiation which is especially important over populous regions, but also plays a role as a potent greenhouse gas. In particular, ozone has a strong potential for radiative forcing in the UT/LS region as well as acting as a UV filter. [10,11] Therefore, the effects of ozone loss in midlatitude regions differ from those at the Poles comprising both actinic and climatic implications.[12]

A catalytic ozone loss cycle involving the formation and solar photolysis of HOCl has been recognised as an important mechanism for mid-latitude ozone loss in the UT/LS:[13]

$ClO + HO_2$	$\rightarrow$	$HOCl + O_2$	(1)
$HOCl + h\nu$	$\rightarrow$	$OH + Cl$	(6)
$Cl + O_3$	$\rightarrow$	$ClO + O_2$	(5)
$OH + O_3$	$\rightarrow$	$HO_2 + O_2$	(7)
Net: $2O_3$	$\rightarrow$	$3O_2$	

The formation of HOCl *via* reaction (1) is significant in not only being the rate determining step in this catalytic cycle (in sunlight) but since this reaction also couples stratospheric chlorine chemistry to tropospheric odd hydrogen (OH and HO_2, denoted HO_x) chemistry. HO_x itself is formed in the stratosphere as a result of wet tropospheric air mixing with dry stratospheric air and the subsequent interaction of water with excited oxygen atoms. This mixing of wet tropospheric air is ordinarily expected not to hydrate the stratosphere through so called 'cold trap' events in which the water vapour rapidly condenses out of the rising air.[14] However, recent studies suggest that these events are rarer than previously believed and that there is a potential moistening of the stratosphere through 'geysers' of ice crystals which pass the tropopause and subsequently sublime.[15] This phenomenon is now believed to be common over tropical regions and may be significant in providing water, and consequently HO_x, up to an altitude of ~20 km.[16]

As a consequence of the importance of chlorine oxide chemistry and odd-hydrogen chemistry in the stratosphere, the ClO + HO_2 reaction is of particular interest. A number of studies have accordingly recently highlighted the importance of the ClO + HO_2 reaction in comparison of atmospheric models with field observations of HOCl.[17,18] Discrepancies between observations and models arising from the differences between the current JPL-NASA recommendation[11] for the temperature dependence of reaction (1) and the rates reported by individual laboratory studies (*e.g.* the initial studies of Stimpfle *et al.*[19]) have been found to have a large impact in the model simulation of HOCl abundances. A study by Anderson *et al.*[20] for example, has also highlighted the potential for significant ozone loss over the US in summertime following deep convective injection of water vapour into the stratosphere. In the mid-latitude regions of the lower stratosphere the dominant source of HOCl is believed to be through gas-phase sources, principally reaction (1) driven by the availability of ClO.[18] Further, a recent study from von Hobe *et al.*[21] has found evidence for significant heterogeneous chlorine activation in the tropical UT/LS, the importance of which is directly dependent upon the rate of the ClO + HO_2 reaction. In order to quantify this in models, knowledge of the kinetics of reaction (1) are important in determining abundances of HOCl and therefore the amount in which the cycle contributes to overall observed ozone losses at mid-latitudes.

There are a number of previous laboratory studies of the ClO + HO_2 reaction, reporting ambient (T = 298 K) temperature rate constants that range between k_1 = (3.8 – 8.26) × 10^{-12} cm^3 $molecule^{-1}$ s^{-1} (Figure 1). However, when considering the reported uncertainties in these determinations, there is reasonable agreement between the studies with the exception of those of Reimann and Kaufman[22] (discharge-flow/resonance fluorescence over p = 2 – 3 Torr at T = 298K), Leck *et al.*[23] (discharge-flow/mass-spectrometry over p = 2 – 6 Torr, T = 298K) and Burrows and Cox[24] (molecular modulation/ultraviolet absorption at p = 760 Torr, T = 300K). Therefore the current JPL-NASA[11] and IUPAC[25] 298K recommendations, based on the average of the ambient temperature data of Hickson *et al.*[26] (discharge-flow resonance-fluorescence at p = *ca.* 1.5 Torr, over the temperature range T = 220 – 336K), Nickolaisen *et al.*[27] (flash photolysis /ultraviolet absorption over p = 50 – 700 Torr, T = 203 – 364 K), Knight *et al.*[28] (discharge-flow/mass-spectrometry over p = 1.1 – 1.7 Torr, T = 215 – 298 K), and Stimpfle *et al.*[19] (discharge-flow/laser magnetic resonance over p = 0.8 – 3.4 Torr, T = 235 – 393 K) (NASA) and Stimpfle *et al.*[19], Cattell and Cox[29] (molecular modulation/ultraviolet absorption over p = 50 – 760 Torr at T = 308 K) , Nickolaisen *et al.*[27] and Knight *et al.*[28] (IUPAC) are in agreement. Of the results of studies shown in Figure 1, Cattell and Cox[29] and Nickolaisen *et al.*[27] performed experiments as a function of pressure from p = 50 – 760 Torr. Neither of these studies found any significant trend in k_1 with pressure implying there is pressure independence in the ClO + HO_2 reaction. Accordingly, when the data are grouped into low pressure studies (p < 50 Torr)[19,22,23,28] and high pressure (p > 50 Torr) [24,27,29] and averaged, there appears to be little difference when considering the combined substantial uncertainties.

The earliest kinetic study of ClO + HO_2 by Stimpfle *et al.*[19] found a strong negative temperature dependence and – interestingly – recorded non-Arrhenius behaviour for k_1 at lower temperatures; which was attributed to complex formation involving a third body in the reaction mechanism. No other subsequent study of the ClO + HO_2 has observed this phenomenon, however the results from the two other studies performed at similarly low pressures may not rule this out. Knight *et al.*[28] do not agree on the sign of the temperature dependence recorded by the Stimpfle *et al.*[19] study while the relatively large uncertainty associated with the Arrhenius expression obtained by Hickson *et al.*[26] encompasses all of the previously published Arrhenius parameters reported for this reaction. This highlights the appreciably poor agreement between the

temperature dependent studies which is illustrated in Figure 2. Apart from the findings of Knight *et al.*[28], it is generally agreed that the ClO + HO_2 reaction exhibits a negative temperature dependence, although the extent of which is unclear, *i.e.* the value of *E/R* varies considerably between each study. Consequently, between the four previously reported temperature dependence studies, the temperature dependence ranges from strongly negative and non-linear (Stimpfle *et al.*[19]), to slightly positive (Knight *et al.*[28]) with Hickson *et al.*[26] and Nickolaisen *et al.*[27] reporting *E/R* values in between. The values of k_1 reported by Nickolaisen *et al.*[27] lie closest to the average of these four studies from which JPL NASA[11] has based their current recommendation. Such values and recommedations for k_1 rely entirely on laboratory studies. However, field observations have also been recently used to attempt to constrain the ClO + HO_2 rate constant.[30] The Submillimeter Wave Limb-Emission Sounder (SMILES) detected ClO, HO_2 and HOCl along a limb of the stratosphere, determining a rate constant for reaction (1) at T = 245 K in keeping with recommendations from laboratory measurements.

The ClO + HO_2 reaction is radical terminating with two reported channels:[11]

$$ClO + HO_2 \rightarrow HOCl + O_2 \quad (1a)$$

$$\rightarrow HCl + O_3 \quad (1b)$$

Experimentally it is found that reaction (1a) appears dominant (>95 %) with reaction (1b) contributing to a maximum of < 5 % of the total reaction yield at temperatures below T = 250 K[31] and even lower at room temperature (0.3 – 2 %)[23,28,32]. Aside from HOCl, there is no direct evidence of any other product formation from reaction (1) between T = 210 – 300 K.

These product studies are supported by the extensive computational studies performed which a detailed review of can be found in Hickson *et al.*[26] In general, the computational studies show that the ClO + HO_2 reaction predominantly follows a direct H-abstraction pathway on the triplet potential energy surface through a weakly hydrogen bonded complex, forming HOCl + $^3O_2$ as the sole product at T = 298 K. At lower temperatures, complex formation through two possible stable isomers of HO_2OCl through a termolecular process is also predicted to occur on the singlet

potential energy surface. These intermediates are thereafter expected to produce OH + ClOO; HCl + $^1O_3$; HOCl + $^1O_2$ and OH + OClO products upon dissociation *via* multistep processes. The findings of the most recent theoretical study, from Zhu *et al.*[33] further support the previous theoretical work and these authors were also able to estimate rate constants for both the total rate constant and also the relative importance of the direct H-abstraction pathway *vs* the stabilization of the potentially stable HOOOCl intermediate which might be expected to be strongly pressure dependent. For the total rate constant, there is general agreement from the computational studies with the experimental data of the previous temperature dependent studies albeit given the error bounds of the recommendation for this rate constant as a function of temperature.

Given the importance of the ClO + HO_2 reaction in (particularly) mid-latitude ozone loss and the considerable uncertainty in k_1 as a function of temperature, the current work aimed to determine k_1 as a function of temperature, using an experimental system uniquely suited to unequivocal monitoring of ClO radicals as demonstrated by, for example, Ferracci and Rowley.[34]

2. Experimental

2 (i) Principles of the experiment

The ClO + HO_2 reaction was studied using laser flash photolytic radical generation coupled with time-resolved ultraviolet absorption spectroscopy for radical monitoring, described in detail below. In this work, ultraviolet absorption was monitored using a charge-coupled-device (CCD) detector[35] which enabled simultaneous wavelength and rapid time-resolved recording of the analysis radiation passed through the photolysed gas mixture. This allowed the accurate and unambiguous determination of ClO radical concentrations as a function of time using 'differential' spectroscopy, also discussed below. The principle of these experiments was that ClO radicals were principally initially generated from reactions of photolytically generated chlorine atoms. In subsequent experiments, the addition of methanol vapour to the precursor gas mixture led to a competition for photolytically produced Cl atoms which, in the presence of excess oxygen, thereafter produced HO_2 radicals rapidly and stoichiometrically, as confirmed by kinetic and analytic modelling, discussed below. The perturbed ClO signal under these conditions, showing a lower initial ClO concentration (attributed to HO_2 production) and a faster decay of the ClO radicals (attributed to the ClO + HO_2 reaction) then exhibited sensitivity to the ClO + HO_2 reaction, which was analysed to extract kinetic parameters. The sensitivity of these parameters to all other kinetic parameters, absorption cross-sections and precursor concentrations was also quantified.

2 (ii) Experimental

The apparatus for this work has been described in detail previously[35] and is summarized briefly here. Precursor gas mixture concentrations were first designed using numerical integration simulations of the expected immediate post-photolysis chemistry, to ensure prompt and exclusive radical formation. Gas mixtures were prepared, in a continuous flow of either nitrogen, oxygen or synthetic air, using flows of precursor gases determined by mass flow controllers (MKS). For corrosive chlorine gas (supplied as diluted, 5% in nitrogen), flows were controlled using a PTFE needle valve and measured using a glass ball flowmeter. For the introduction

of methanol vapour, a flow of nitrogen was passed through a bubbler containing liquid methanol held at a known and constant temperature, $T = 0$ °C, in an ice/ water bath. All flow controllers and meters were routinely calibrated. The total flow rate of gases (typically 1000 standard $cm^3\ min^{-1,}$ with a cell volume of 178 cm^3) was such that the flowout of species from the reaction vessel during an experiment was negligible on the timescale of the kinetic processes under study, and was in any case accounted for in the analytic procedures. The precursor gas mixture was delivered, *via* PTFE tubing, to a double jacketed reaction vessel, 1 m in length, which was temperature controlled by recirculating perfluoroether fluid (Galden HT180) supplied from a thermostat unit (Huber CC180). The temperature of the gas mixture within the reaction vessel was controlled within a precision of ± 0.5 K, and the accuracy of the gas temperature was calibrated in separate experiments.[36] The outer jacket of the reaction vessel was evacuated for thermal insulation. Similarly, evacuated double-windowed end pieces on the reaction vessel allowed coupling of the photolysis laser beam and the analysing UV radiation through the reaction vessel without window condensation effects. Reactions in this work were all performed at ambient atmospheric pressure, (p = 760 ± 20 Torr) as measured using a capacitance manometer (MKS Baratron).

Radicals and atoms were generated in the reaction vessel using laser photolysis. The output from a XeF excimer laser, operating at 351 nm, (Lambda-Physik COMPex 201) was collimated and expanded using fused silica cylindrical lenses and then coupled longitudinally through the reaction vessel using dichroic mirrors (Exitech). The photolysing laser beam was expanded to completely fill the internal volume of the reaction vessel and, after passing through the reaction vessel, was coupled out into a beam dump/ Joulemeter (Lambda-Physik). The attenuation of the photolysis laser beam by the optics and the absorbing precursor gases within the reaction vessel was always kept below 30%, precluding significant concentration gradients of photolytically generated species, which might otherwise have distorted kinetics as observed along the length of the reaction vessel. The typical laser pulse energy was 80 – 100 mJ/ pulse, delivered in *ca.* 20 ns.

As discussed above, species in the reaction vessel were monitored using time resolved ultraviolet absorption spectroscopy. The source for UV absorption was a 75 W xenon arc lamp (Hamamatsu C6979), output from which was collimated using fused silica lenses and passed once through the reaction vessel, counterpropagating the photolysis laser beam, before being focussed into the detection system. The UV analysing beam (typically 10 mm in diameter) always sampled a volume of gas within the photolysis beam (14.8 mm in diameter – that of the reaction vessel).

The analysing UV radiation transmitted through the gas mixture was focussed onto the entrance slit of a 0.25m focal length Czerny-Turner spectrograph (Chromex 250IS). The spectrograph was fitted with toroidal mirrors, to maintain the vertical focus of the analysed light, and was operated with a 600 lines/mm diffraction grating. Light output from the spectrograph was imaged onto the top 31 rows of pixels of a two-dimensional 1152 (rows) × 298 (columns) charge-coupled-device (CCD) detector array (Wright Instruments). The remaining rows of the CCD array were optically masked. The light incident on the CCD array was converted into photocharge and stored in a potential well within each pixel. Subsequently, by application of phased voltages to parallel transfer electrodes across the array, it was possible to rapidly and efficiently transfer signal, row by row, along the long axis of the array, out of the illuminated region of the device. In this way, sequential transmission spectra of the investigated gas mixture could be recorded on timescales as fast as 1 μs/ spectrum (but otherwise arbitrarily slowly). A mechanical shutter prevented buildup of photocharge (signal) between experiments. Transmission spectra could then be read out for subsequent analysis following transfer of the entire signal across each row of the array.

2.(iii) Radical formation

ClO radicals were generated following laser photolysis of Cl_2/ Cl_2O mixtures in nitrogen, oxygen or synthetic air carrier gas. The Cl_2O was generated *in situ* using the method initially described by Hinshelwood and Pritchard:[37] a known flow of Cl_2 was passed through a trap containing dried mercuric (II) oxide.

$$2Cl_2(g) + HgO(s) \rightarrow Cl_2O(g) + HgCl_2(s) \quad (8)$$

The principal source of ClO radicals thereafter resulted from the photolysis of molecular chlorine and the subsequent reaction of Cl atoms with an excess of dichlorine monoxide, Cl_2O:

$$Cl_2 + h\nu \rightarrow 2\,Cl \quad (9)$$

$$Cl + Cl_2O \rightarrow Cl_2 + ClO \quad (10)$$

Direct photolysis of Cl_2O also contributed a minor source of ClO, given the smaller cross-section of Cl_2O compared to Cl_2 at the 351nm photolysis laser wavelength (σ_{Cl_2} (351nm) = 1.8×10^{-19} $cm^2 molecule^{-1}$, σ_{Cl_2O} (351nm) = 7.0×10^{-21} cm^2 $molecule^{-1}$) .[11]

For the generation of HO_2, chlorine atoms were reacted (competitively) with an excess of methanol vapour, in the presence of a large excess of molecular oxygen:

$$Cl + CH_3OH \rightarrow HCl + CH_2OH \quad (11)$$

$$CH_2OH + O_2 \rightarrow HCHO + HO_2 \quad (12)$$

Typical precursor concentrations were: $[Cl_2] = 2.5 - 5.0 \times 10^{16}$ molecule cm^{-3}; $[Cl_2O] = 1.5 - 5.0 \times 10^{15}$ molecule cm^{-3}; $[CH_3OH] = 0.4 - 1.1 \times 10^{16}$ molecule cm^{-3} with the carrier gas balanced to 1 atm. These concentrations were such that photolytically generated Cl atoms were always rapidly (on the timescale of subsequent chemistry) and stoichiometrically consumed to produce either ClO or HO_2 radicals. Typical initial (immediately post-photolysis) radical concentrations were in the range $(1 - 2) \times 10^{14}$ molecule cm^{-3}.

Experiments were performed recording time resolved spectra before, during and after laser photolysis over a total timescale of 15 – 100 μs/ experiment. These spectra were recorded over a wavelength range of 262.9 – 296.2 nm, at a spectral resolution of 0.8 nm full width half-maximum (FWHM). Wavelength calibration and spectral resolution were verified in separate experiments recording the emission spectrum

from a mercury 'pen-ray' lamp. Typically, 20 – 50 photolysis experiments were conducted and the results co-added, for each determination of k_1, and at least six determinations were conducted at each experimental temperature. Analytical procedures, and sensitivity analyses are discussed below.

2.(iv) Data analysis

The data recorded by the CCD consisted of a matrix of 1152 (rows) × 298 (columns) of signal representing transmitted intensity through the reaction vessel. Each row of data therefore corresponded to a transmission spectrum at a particular time, each column to a time resolved transmission at a particular wavelength. Data were recorded continuously before, during and after laser photolysis. Recorded transmissions were converted into wavelength and time resolved absorbances, $A_{\lambda,t}$, relative to the pre-photolysis transmitted intensities using Beer's Law:

$$A_{\lambda,t} = \left\langle I_{\lambda,0} \right\rangle \Big/ I_{\lambda,t} \qquad \text{(i)}$$

Where $\langle I_{\lambda,0} \rangle$ is the *average* pre-photolysis transmitted light intensity at wavelength λ and $I_{\lambda,t}$ is the transmitted light intensity at wavelength λ and time t. The recorded absorbances therefore exhibit *changes* in absorption brought about by laser photolysis and subsequent gas phase chemistry.

2. (v) Determination of ClO concentrations

The concentration of ultraviolet absorbing species in the reaction vessel is related to absorbance by the Beer-Lambert law:

$$A_{\lambda,t} = \sum_i \sigma_{\lambda,t}.[\mathrm{i}]_t.l \qquad \text{(ii)}$$

Where $A_{\lambda,t}$ is the absorbance at a wavelength λ and time t, $\sigma_{\lambda,t}$ is the absorption cross-section of absorbing species i at wavelength λ and l is the optical path length through the reaction mixture. This product is summed over the number of absorbers, i, present.

In the present work, over the wavelength range covered, several UV absorbing species, including precursor gases, radicals and reaction products were present. For many of these species, the UV absorption spectra are spectrally structureless, and whilst in principle their contributions to total absorption could be deconvoluted, in practice the similarities in the spectra precluded this, even with broadband spectral monitoring. By contrast, ClO radicals exhibit distinctive spectral structure attributed to the ($A^2\Pi \leftarrow X^2\Pi$) vibronic transition.[11] This structure was exploited to determine ClO concentrations using 'differential' spectroscopy. In this procedure, the recorded absorption spectrum exhibiting the ClO spectral structure is high-pass filtered. A suitable reference spectrum of ClO is then analogously filtered and the filtered spectrum fitted to the experimental spectrum, minimising the sum of squares of residuals to determine the ClO species concentration using the Beer Lambert law (ii), and as described in detail previously.[38] In this way, the ClO concentration as a function of time could be accurately and unequivocally extracted from the time resolved spectra recorded on the CCD, despite the presence of many other absorbing species in the spectral window studied. Critical to this spectral fitting is that the instrumental resolution adopted is that at which the ClO absorption cross-sections are available, since the ClO cross-sections are a strong function of instrumental resolution. In this work, a spectral resolution of 0.8 nm FWHM was chosen, as verified by recording and Gaussian fitting to peaks in the emission spectrum from a mercury 'pen-ray' lamp. This resolution is identical to that employed by Ferracci and Rowley[34] and Boakes *et al*.[38] from which the extensively studied ClO absorption cross-sections, and their temperature dependence were taken. The temperature dependent 'differential' absorption cross-sections for the representative 12-0 vibronic band of ClO, corresponding to the difference between the peak at 275.2 nm minus the trough at 276.4 nm were given by:

$$\sigma_{ClO\ diff}/\mathrm{cm^2\ molecule^{-1}} = (1.07 \pm 0.33) \times 10^{-17} - \left\{(2.46 \pm 1.1) \times 10^{-20}.(T/\mathrm{K})\right\} \quad \text{(iii)}$$

Whilst these two wavelengths were used at which to quantify the ClO differential absorbance, it should be noted that a spectrum recorded over the entire range *ca.* 260 – 296 nm was recorded at *each* time point, and the spectral fitting adopted all of this range in determining $[ClO]_t$.

3. Results and kinetic analysis

3. (i) Temporal profiles of [ClO] recorded in the absence or presence of CH_3OH

A typical time-averaged post-photolysis (relative to pre-photolysis) absorption spectrum recorded from a $Cl_2/Cl_2O/$ carrier gas mixture is shown in Figure 3. The distinctive spectral structure of ClO is apparent and the fit of the calibrated differential reference spectrum along with the residuals confirmed the fitting of the ClO signal and the extraction of ClO concentrations. Also shown in Figure 3 is the analogous spectrum recorded under identical conditions except for the inclusion of methanol vapour (in this case 1.1×10^{16} molecule cm^{-3}) showing a clear reduction in the average ClO absorbance.

From fitting to each time resolved absorption spectrum recorded throughout a given experiment, two temporal profiles of ClO radical concentration, recorded in the absence of methanol, are shown in Figure 4a. Also shown is a temporal profile of ClO recorded in the presence of methanol, which was obtained in an experiment carried out intervening those without CH_3OH present, under otherwise identical conditions. This clearly shows that the initial post photolysis ClO concentration is reduced in the presence of methanol, but recovers almost exactly to its original level in the subsequent experiment once the source of methanol has been removed. Figure 4a also shows kinetic fits to the ClO traces recorded in the absence of methanol. These fits were based solely upon the analytical solution to a 2-reaction model involving the termolecular association of ClO radicals (reaction (2)) and the thermal decomposition of Cl_2O_2 (reaction (−2).[38]) The fitting optimised the initial post photolysis concentration of ClO, but also accounted for a temporal averaging inherent to the illumination of multiple rows on the CCD detector.[34] The forward and reverse reaction rate constants k_2 and k_{-2} were also optimised.

The derived values of k_2 and k_{-2} derived from these particular fits to individual experiments were $(4.35 \pm 0.05) \times 10^{-13}$ cm^3 $molecules^{-1}$ s^{-1} and (40.4 ± 0.44) s^{-1} respectively (initial experiment), and $(4.27 \pm 0.05) \times 10^{-13}$ cm^3 $molecules^{-1}$ s^{-1} and (40.1 ± 0.44) s^{-1} respectively (post-methanol experiment) at $T = 298$ K, $p = 760$ Torr (*i.e.* at a total number density of 2.38×10^{19} molecules cm^{-3}). Similarly the initial

ClO concentrations derived from these fits lay within ~ 3 % of each other. The ensemble of kinetic parameters recorded in the absence of methanol vapour are described below and reported in Table 1. These parameters are also compared, in Table 1, with those calculated from the current NASA-JPL data evaluation[11] indicating reasonable agreement.

Given the robustness of the self-reaction kinetics of ClO obtained in experiments with results such as shown in Figure 4a, a simulation of a ClO temporal profile with identical kinetic parameters k_2 and k_{-2} but with a lower $[ClO]_0$, re-optimised for the intermediary experiment in the presence of methanol is shown in Figure 4b. Clearly, the observed kinetics of ClO decay are no longer reproduced by a ClO reversible dimerization-only scheme. Further, even allowing the kinetic parameters for k_2 and k_{-2} to subsequently vary within the model to optimise the fit could not reproduce the form of the observed ClO temporal behaviour, and in any case led to rate coefficients for ClO association which gave significantly enhanced kinetic values for the forward dimerization reaction rate constant k_2, incompatible with any known third body enhancement for ClO association which may have resulted. Another reaction is clearly operating in the presence of methanol.

A series of analogous experiments were therefore carried out monitoring ClO in the absence of methanol, but intervening with methanol present over a range of methanol concentrations (between $(0.41 – 1.13) \times 10^{16}$ molecule cm^{-3}). After each addition of methanol, an experiment was performed in which the methanol vapour trap was by-passed to revert to pure Cl_2/Cl_2O photolysis. A selection of the resulting ClO temporal traces is presented in Figure 5. The maximum [ClO] concentrations recorded in these experiments are presented in Table 2, and again confirm the reproducibility of the ClO concentration in the absence of methanol and a systematic dependence of the maximum ClO concentration as a function of added methanol concentrations in the intervening experiments.

The initial rates of loss of ClO radicals were also calculated for ClO temporal traces such as those shown in Figure 5. These are also presented in Table 2 and shown graphically in Figure 6. Again this demonstrates the enhanced loss rate of ClO,

despite the lower initial ClO concentrations, when methanol, in the presence of excess oxygen, is introduced to the reaction mixture.

The inference from the analysis of the ClO temporal traces recorded in the presence of methanol, and confirmed by numerical modelling, is that the reduction in $[ClO]_0$ is due to competitive loss of chlorine atoms with methanol (reaction (11)), and that in the presence of a large excess of oxygen this competitive reaction produces HO_2 radicals stoichiometrically through reaction (12). This assumption was investigated in more detail by considering the branching of Cl atom reactions with Cl_2O or with methanol as a function of methanol concentration. The maximum [ClO] clearly decreases as methanol concentration is increased, as shown in Figure 7. This behaviour was readily fit by a simple model optimising the initial radical concentrations and either the competitive rate constants for Cl atoms, or the precursor concentrations of Cl_2O or methanol. The Cl + methanol rate constant returned from this analysis was greater than that reported in the literature (*ca.* 2×10^{-10} cm^3 $molecule^{-1}$ s^{-1}) at T = 298 K, or the methanol concentration was lower than anticipated. Nonetheless these studies confirmed, through an analysis of the Cl atom lifetimes, that the 'missing' Cl and therefore ClO, which was entirely restored on removing methanol, was entirely due to the Cl + CH_3OH reaction, and in the presence of a large excess of oxygen, the subsequent generation of HO_2.

The ClO traces recorded in the presence of methanol were therefore analysed using a variety of assumptions, discussed below.

3. (ii) Analysis of the [ClO] temporal profiles recorded in the presence of methanol

Most simplistically, as discussed above, the reduction in the initial post-photolysis ClO concentration upon the addition of methanol to the system could be assigned to a rapid and stoichiometric production (from Cl atoms, *via* reactions (11) and (12)) of HO_2 radicals. Thus, for analysis of these temporal traces, the total radical concentration was fixed in the numerical model, the $[ClO]_0$ concentration reoptimised to fit to that of the observed ClO trace and the initial HO_2 concentration therefore effectively stipulated in the model. An additional (terminating) reaction, that of ClO + HO_2, was incorporated into this model, and its rate constant optimised. The

resulting fits from this analysis at T = 298 K are shown in Figure 4a. A consistent ClO + HO_2 rate constant is obtained from this analysis except at the highest methanol concentrations used when HO_2 is in excess over ClO. This result is unsurprising, since this initial analysis does not account for the known self-reaction of HO_2 radicals and which will become increasingly significant as $[HO_2]_0$ is increased.[36] This analysis does however demonstrate further that the inclusion of methanol and excess oxygen to the reaction system is consistent with the formation of (a self-reacting radical such as) HO_2 and an additional termination reaction for ClO radicals.

A second analytical method wherein the initial concentrations of ClO and HO_2 were allowed to vary in optimising the fits to ClO traces was also carried out. In this case, the fits to data were equally good as previously, and the rate constants at high $[ClO]_0$/ $[HO_2]_0$ ratios were remarkably consistent with the results from analysis constraining the total radical concentration. In this case, the rate constant enhancement at low $[ClO]_0$/ $[HO_2]_0$ ratios was not as significant as in the preceding analysis, but rather the total radical concentration indicated an apparent shortfall of radicals compared to the expected total concentration inferred from experiments carried out without methanol. Again this implies a significant loss of HO_2 through the known HO_2 self-reaction.

These initial analytic procedures, whilst simplistic, gave considerable insight into the nature of the reactive system employed and the flux of photolytically generated atoms and radicals through the various potential channels, which was supported by numerical integration. In light of this, a more comprehensive analysis was carried out, using a model with all known gas phase chemistry, physical processes such as gas flowout from the reaction vessel, and a degree of constraint on the data fitting as discussed after consideration of the provenance of radicals, discussed below. Details of this model are presented in Table 3.

3. (iii) Analysis of radical production routes

The total concentration of the chlorine containing species (Cl_2 and Cl_2O) in the precursor gas mixture was governed by the flow rate of (diluted) Cl_2 into the carrier flow, and the degree of conversion of Cl_2 into Cl_2O upon passing through the trap containing mercuric oxide (reaction (8)). With the entire flow of Cl_2 passing through

the trap, this conversion was typically high (70 – 80% removal of Cl_2) as confirmed by spectroscopy.[34] In practice, a degree of control (reduction) over this conversion was afforded using a tube bypassing the HgO trap, flow through which was controlled by a PTFE needle valve.

If the fractional conversion of Cl_2 into Cl_2O in the precursor gas arrangement is defined as α, and the total concentration of Cl_2 introduced to the system, as determined from calibrated flow rates is $[Cl_2]_{total}$ (the concentration of Cl_2 that would be present in the *absence* of mercuric oxide), then the actual initial concentrations of Cl_2O and Cl_2 in the precursor gas mixture may be expressed as:

$$[Cl_2]_0 = (1-\alpha)\,[Cl_2]_{total} \qquad \text{(iv)}$$

$$[Cl_2O]_0 = (\alpha/2)\,[Cl_2]_{total} \qquad \text{(v)}$$

(taking account of the stoichiometry of the Cl_2 to Cl_2O in reaction (11)).

Upon laser photolysis, the initial (immediate post-photolysis) concentrations of Cl atoms and ClO radicals, from the photolysis of Cl_2 and Cl_2O (which yields exclusively Cl + ClO at $\lambda = 351$ nm[11] are then given by:

$$[Cl]_0 = 2f(Cl_2)\,[Cl_2]_0 + f(Cl_2O)\,[Cl_2O]_0 \qquad \text{(vi)}$$

$$[ClO]_0 = f(Cl_2O)\,[Cl_2O]_0 \qquad \text{(vii)}$$

Where $f(Cl_2)$ and $f(Cl_2O)$ are defined as the respective fractions of the Cl_2 and Cl_2O gases photolysed.

Subsequently, in the absence of methanol, and with Cl_2O in excess, all of the initial photolytically generated Cl atoms react rapidly and exclusively with Cl_2O forming ClO in reaction (13) where $k_{14}(T = 298\ K) = 9.6 \times 10^{-11}$ molecule^{-1} cm^3 s^{-1}.[11] Thus, the effective instantaneous concentration of ClO radicals directly after laser photolysis is in this case given by:

$$[ClO]_0 = 2\,f(Cl_2)\,[Cl_2]_0 + 2\,f(Cl_2O)\,[Cl_2O]_0 \qquad \text{(viii)}$$

Which from (iv) and (v) gives

$$[ClO]_0 = \{[2\,f(Cl_2)\,(1-\alpha)] + [f(Cl_2O)\,\alpha]\}[Cl_2]_{total} \qquad \text{(ix)}$$

Now, assuming that the ratio of the fractional photolyses of Cl_2 and Cl_2O in the precursor gas mixture is equal to the ratio of the absorption cross-sections of these species at the laser wavelength of 351 nm (this is the case since the photolysis quantum yield for both molecules are unity at 351 nm[11]), the immediate post photolysis ClO concentration may be expressed as

$$[ClO]_0 = \{[2\,\beta\,f(Cl_2O)\,(1-\alpha)] + [f(Cl_2O)\,\alpha]\}[Cl_2]_{total} \qquad \text{(x)}$$

where β is defined here as $\{f(Cl_2)/f(Cl_2O)\} = \{\sigma(Cl_2)/\sigma(Cl_2O)\}_{\lambda=351nm}$
leading to $\beta = 8.53 \times 10^{-2}$ from the latest NASA evaluation.[11]

Thus, measurement of the immediate post photolysis concentrations of ClO, provided by kinetic fitting to the ClO temporal traces recorded in the absence of methanol, constrains $f(Cl_2O)$ and therefore, from β, $f(Cl_2)$ for a given value of the Cl_2 to Cl_2O conversion, α. Given that α was also constrained separately, through independent measurements of the Cl_2 and Cl_2O absorption spectra in the precursor gas mixture, experiments carried out in the absence of methanol therefore gave considerable insight into the initial Cl atom and ClO radical concentrations immediately post photolysis.

Upon the introduction of methanol into the precursor gas mixture, in experiments that intervened those without methanol, the methanol competes with Cl_2O for the initial photolytically generated Cl atoms, *via* reaction (14). In the presence of excess oxygen, the CH_2OH radicals then react rapidly and exclusively to generate HO_2 radicals in reaction (15), thereby leading to prompt HO_2 formation along with the ClO radicals, immediately post photolysis.

Furthermore, given the parameters extracted in equation (x) from the experiments conducted in the absence of methanol, the immediate post photolytic concentration of HO_2 could be inferred, along with that of ClO, which was directly measured.

3. (iv) Analysis of ClO temporal traces recorded in the presence of methanol

The ClO temporal traces recorded in the presence of methanol vapour were analysed through fitting of a simulated ClO profile based upon the model presented in Table 3. The initial post photolysis ClO concentration, and the rate constant for the ClO + HO_2 reaction were varied to optimise the fit, along with a third parameter, δ, which effectively partitioned the modelled initial Cl atom and ClO radical concentrations as described by equations (iv) and (v), along with the constraint to these concentrations provided using the parameter β and expressed by equation (x). In this way, the only varied parameter in addition to the initial radical concentration and the ClO + HO_2 rate constant was effectively the parameter α, the fractional conversion of Cl_2 to Cl_2O, which reflected the efficacy of the HgO trap and the degree to which it was bypassed in the gas flow which was specific to a given experiment.

The parameters extracted from the analysis of the ClO traces recorded in the presence of methanol are summarised in Table 4. The initial post photolysis concentrations of ClO, *i.e.* $[ClO]_0$, reflected the competition for chlorine atoms between methanol and Cl_2O according to the current JPL-NASA recommendations for these rate coefficients as a function of temperature.[11]

The rate constants for the ClO + HO_2 reaction obtained in this work are shown in Arrhenius form in Figure 2, along with results from previous studies of this reaction. The results show a negative temperature dependence for the overall rate constant, with linear Arrhenius behaviour, described by:

$$k_1 = \left(1.74\ ^{+1.56}_{-0.83}\right)\times 10^{-12}\exp\left(\frac{474 \pm 161}{T/\mathrm{K}}\right)\mathrm{cm}^3\ \mathrm{molecule}^{-1}\ \mathrm{s}^{-1} \qquad \text{(xi)}$$

where errors are 1 σ, from the Arrhenius fit to all data.

In principle, given the nature of the broadband UV absorption spectroscopy adopted in this work, the time resolved concentrations of HO_2, in addition to those of ClO, could have been monitored, albeit requiring a wider spectroscopic wavelength range. However, in practice, the presence of several strongly absorbing species in the reaction mixture (Cl_2O, ClO, Cl_2O_2) and the absence of any distinctive spectral structure for the absorptions of these species, or indeed for HO_2, precluded this monitoring. Thus, the HO_2 concentrations were inferred as discussed above. A detailed sensitivity analysis was therefore also performed to examine the integrity of these assumptions, and to quantify the potential effect of uncertainty in the kinetic and physical parameters used in the analytic model, as discussed below

4. Discussion

4. (i) Sensitivity analysis

To investigate the sensitivity of the ClO + HO_2 rate constant, k_1, extracted from the ClO traces recorded from Cl_2O/ Cl_2 photolysis in the presence of methanol vapour and excess oxygen, the analytic model used was systematically perturbed and the effect on the value of k_1 and δ recorded. Specifically, each of the rate constants for the chemistry summarised in Table 3 were altered, in turn, by ± 50 % in the model, and the perturbed model used to re-evaluate the rate constant for ClO + HO_2 from representative traces, at T = 298 K, and at T = 210 K, *i.e.* the upper and lower limit of the temperature range over which this reaction was studied. In a similar fashion, potential uncertainties in the absorption cross-sections of ClO radicals (taken from the parameterisation used by Ferracci and Rowley[34]) were considered, as discussed below. For the majority of reactions included in the model, the perturbation of the rate constant by ± 50% (which is typically somewhat greater than the recommended uncertainty) led to a returned rate constant for ClO + HO_2 within ~ 2 % of that obtained using the unperturbed model at T = 298 K and T = 210 K.

However, there were a few reactions that affected the extracted values of k_1 and/or δ more significantly. Starting at T = 298 K, perturbing the initial ClO and HO_2 radical formation chemistry significantly affected δ, although k_1 only minimally. For reaction (13), there was a maximum change in the extracted value of k_1 compared the input value of 3 %, whereas a doubling and halving in k_{13} perturbed δ by 25 % and – 14 % respectively. Conversely, for reaction (14) the effect on δ was reversed with the effect on k_1 still minimal. k_1 and δ were also found to be sensitive to the ClO self-reaction: perturbing k_2 increased the extracted k_1 by up to 10 % and δ by 6 %. However k_{-2} had a more pronounced effect on k_1 with the returned values increased by 14 % and 38 % upon doubling and halving k_{-2} respectively and δ was perturbed by a maximum of 10 %.

The rate coefficient of the HO_2 self-reaction:

$$HO_2 + HO_2 \rightarrow H_2O_2 \qquad (13)$$

is also significant in extracting an accurate value of k_1. Overestimating and then underestimating k_{16} by a factor of 2 results in values of k_1 perturbed by 16 % and – 70 % and δ by 10 % and 20 % respectively.

Importantly, HO_2 reacts with methanol (the HO_2 precursor reagent) reversibly to form the $HO_2.CH_3OH$ complex which itself can react further with itself and other HO_2 radicals:[36,39-41]

$$HO_2 + CH_3OH + M \rightleftharpoons HO_2.CH_3OH + M \qquad (14)\ (-14)$$

$$HO_2.CH_3OH + HO_2.CH_3OH \rightarrow \text{Products} \qquad (15)$$

$$HO_2 + HO_2.CH_3OH \rightarrow \text{Products} \qquad (16)$$

This chemistry can lead to an enhancement in the observed rate coefficients for reaction (16). However, the kinetic model used in this work incorporates the Stone and Rowley[36] parameterisation for k_{16}, including the methanol enhancement. At T = 298 K, it was found that excluding the methanol enhancement of k_{16} had a minimal effect on the extracted k_1 and δ, perturbing them by ~ 2 % even, even for simulations that used the maximum experimental $[CH_3OH]$. This is in contrast to the sensitivity analysis carried out for T = 210 K, where the effect of methanol on HO_2 had a large effect on both k_1, returning a value 68 % lower than the input value if unaccounted for. Similarly, perturbing k_{16} by a factor of 2 led to a deviation of up to ± 70 %, showing that the effective rate constant of the HO_2 self-reaction for a given $[CH_3OH]$ is important at the low temperature limit used in this work.

The reaction that affects the extracted value of k_1 most significantly at T = 210 K is k_2, which yields a result that is smaller by a factor of 1000, upon doubling. Doubling k_2 is however an extreme sensitivity condition, given the NASA error limits on this association are +/− 15%. Halving k_2 has a vastly smaller effect, perturbing k_1 by 16 %. The effect on δ is 12 % and 30 % upon doubling and halving k_2 respectively. Again, reactions (11) and (12) affect k_1 by up to 30 % under these conditions. Other

reversible processes that rely on the thermal stabilisation of products, namely the formation of ClOO *via* the reaction of Cl + O_2 and then it's subsequent reaction with Cl_2 becomes more significant at T = 210 K, changing extracted k_1 by up to 10 %.

A subsequent flux analysis of the principal reactants of the chemical system, ClO and HO_2, showed that the relative importance of these rate constants could be rationalised. This analysis demonstrated that under experimental conditions, the vast majority of ClO and HO_2 formed react almost exclusively *via* reactions (1), (2,–2) and the HO_2 self-reaction. The importance of the ClO or HO_2 self-reaction chemistry in particular, was evidently dependent upon the relative amount of $[ClO]_0$ and $[HO_2]_0$.

For the ClO cross-section sensitivity, alteration of σ_{ClO} to notional upper and lower bounds of uncertainty of 10% as expressed in equation (iii) led to an average change in the extracted rate constant for ClO + HO_2 of *ca.* 25%. This sensitivity was found to be greater at larger $[ClO]_0/[HO_2]_0$ ratios, unsurprisingly as ClO is dominant under such conditions.

Taking all of the sensitivity parameters that have been considered to assess the veracity of k_1 dependent upon uncertainties in chemical or physical parameters, a least squares sum of all sensitivity parameters indicates an uncertainty of *ca.* 26 % at T = 298 K, leading to *ca.* 47% at T =210 K. This however assumes such potential systematic errors are independent of each other.

4. (ii) Assumptions of the kinetic analysis

Aside from the sensitivity to kinetic and spectral parameters discussed above, the fundamental assumption employed in this work was that the photolytically generated Cl atoms produced exclusively ClO in the absence of methanol, which was indeed observed explicitly, but additionally HO_2 radicals, when methanol and excess oxygen were present. This was supported by the analytic calculations presented above along with numerical integration simulations using all known gas phase chemistry[11] and the well-established concentrations of precursor species present. Methanol and oxygen mixtures are commonly used as a source of HO_2 radicals in the presence of photolytically produced Cl atoms.[36] The systematic variation of $[ClO]_0$ with added methanol concentration was also consistent with a competition for Cl atoms either reacting with Cl_2O or CH_3OH. Further, the systematic reproducibility of the ClO temporal traces recorded before and after the addition of methanol vapour in successive experiments also supports the robustness of this chemistry.

In the present study, large concentrations of methanol have been used such that its effect is expected to significantly enhance the observed rate constant of the HO_2 self-reaction, *via* the formation of the methanol hydroperoxy radical complex, $HO_2.CH_3OH$ as discussed above. This species has not been treated as an individual species in our kinetic mechanism but the effect of its presence has been accounted for on the HO_2 self-reaction *via* the application of the Stone and Rowley[36] linear parameterisation of the HO_2 self-reaction methanol dependence. As discussed above, the sensitivity analysis demonstrated that the accuracy of k_1 is dependent on the effective rate of reaction (13), with the effect of methanol becoming important at low temperatures. However, the effect of methanol on determining k_1 was negligible at T = 298 K and the difference between the recommended k_{16} and that of Stone and Rowley is 9 %, which changes the optimised k_1 by no more than 3 %. Although the Stone and Rowley parameterisation has been disputed by Christensen *et al.*[40] in calculating the zero methanol HO_2 self-reaction rate constant, particularly at lower temperatures, the range of $[CH_3OH]$ used in this work leads to similar *effective* rate

constants of HO_2 + HO_2 for both the linear and Christensen *et al.*[40] non-linear parameterisations. Therefore, the secondary effects of methanol on the kinetic analysis of reaction (1) are considered accounted for, assuming $HO_2.CH_3OH$ reacts with ClO at the same rate as HO_2 and there is no effect on ClO self-reaction chemistry from the presence of CH_3OH. This assumption is difficult to test given that the initial ClO to HO_2 ratio is controlled by the levels of methanol.

4. (iii) Comparison with previous work

The present work reports an ambient temperature, T = 298 K, value of k_1 = (8.51 ± 1.54) × 10^{-12} molecules^{-1}cm^{3}s^{-1}, taken from typically six determinations of k_1 at each methanol concentration used and, at this temperature, a total of 8 different methanol concentrations in the range stipulated above. Errors are 1 σ, statistical only. Comparing this to the other previous reports of k_1, shown in Figure 1, this shows that the present work reports the highest average value for k_1 at T = 298 K, albeit within the error limit of several of the previous studies, and particularly in agreement with those studies carried out at high pressure (p > *ca.* 50 Torr).

For the temperature dependence of k_1, shown in Figure 2 in comparison with results of previous work, this study reports a stronger negative temperature dependence (E/R = (– 474 ± 161) K than previously observed, aside from the Stimpfle *et al.*[19] parameterisation, consequently resulting in a greater value for k_1 = (1.70 ± 0.64) × 10^{-11} cm^3 molecule^{-1} s^{-1} at the lowest temperature studied in the present work (T = 210 K). As with the ambient temperature results, the values of k_1, and their temperature dependence, most closely resemble previous determinations of k_1 recorded in experiments conducted at high (p > *ca.* 50 Torr) pressures.

Considering the approach taken for the present work, compared with previous studies, at T = 298 K and as a function of temperature, several studies have also had to rely upon somewhat indirect measurements to infer the concentrations of ClO and/ or HO_2

radicals. Considering first the low pressure (p < *ca.* 50 Torr) studies, the earliest ambient temperature study, that of Reimann and Kaufmann[22] detected HO_2 following its conversion to OH (*via* reaction with NO) and subsequent laser induced fluorescence of OH. As subsequently noted and accounted for in the analysis by Hickson *et al.*,[26] this procedure may be compromised by a reduction in stoichiometry in this conversion as a result of, for example, secondary chemistry of HO_2 such as the HO_2 self-reaction or heterogeneous losses of radicals which are endemic to flow tube studies and which therefore have to be accounted for. In the Reimann and Kaufmann study, the concentrations of ClO were also not directly measured, but obtained from inference and extrapolation of the Cl atom signal recorded. In similar fashion, the study of Leck *et al.*,[23] which used mass spectrometric detection of species sampled from a flow tube, inferred ClO radical concentrations from the depletion of the precursor species Cl_2 when the microwave discharge used to generate radicals was operated.

Considering the high pressure ensemble of ambient temperature studies of k_1, those of Burrows and Cox[24] and Cattell and Cox[29] used continuous photolysis of precursor gas mixtures in one case analogous to those used in the present work, Cl_2 with Cl_2O[24] and in the other with a chlorine, hydrogen, oxygen mixture[29] to generate radicals. This photolysis was modulated over several seconds and UV spectroscopy was used to monitor a composite radical and product signal, which was then fitted using numerical integration to extract the value of k_1. This approach, whilst noteworthy and pioneering, does however carry the risk that not only the initial reactants but then the subsequent products may be photolysed, leading to extensive and potentially complex secondary chemistry and a subsequent reduction in sensitivity to the reaction of interest. Further, the single wavelength UV absorption monitoring gives a time-resolved signal containing contributions from all potential UV absorbing species present. By contrast, Nickolaisen *et al.*[27] employed pulsed flashlamp photolysis/ ultraviolet absorption to monitor (principally) HO_2 (at λ = 210 nm) and ClO (in a dual

wavelength set-up at λ = 275.2 nm and λ = 276.4 nm) from a variety of precursor sources including (F_2, H_2, O_2, Cl_2O) and (Cl_2, Cl_2O, CH_3OH, O_2) in common with the present work. The recorded absorbance traces obtained at λ = 210 nm were modelled to infer the HO_2 concentration, in the presence of a number of other absorbing species. The differential signal at the two higher wavelengths was used as a direct measure of the ClO absorbance.

Comparison of this work to previous, analogous studies, notably that of Niclolaisen *et al.*, invites examination. In the present work, only a single radical, ClO, was monitored, *but* over a broad wavelength range that permits differential spectroscopy, complete spectral fitting and thereafter unequivocal ClO radical concentration determination. Nickolaisen *et al.*[27] adopted a dual wavelength absorption approach to monitor ClO, which evidently provides an improved marker for ClO over single wavelength monitoring, but, as recognised by Boakes and Rowley[38], may contain inherent risks in the case of high resolution peaks and troughs of absorption showing a massive sensitivity to very small potential wavelength variations during the course of the experiment, which are commonplace. The third single wavelength employed by Nickolaisen *et al.*, 210 nm also presents potential sensitivity issues, as absorbance at this wavelength is not in any way a unique signal for the HO_2 concentration. Many of the radical precursors and reaction products absorb considerably at 210nm. Many of the cross-sections for such species are uncertain, and the subsequent deconvolution of the 210 nm temporal absorbance could be compromised to an extent by such contributions. Thus, whilst the study of a mixed radical reaction might be expected to be improved by monitoring of the two reacting partners, the current study aims to show that unequivocally monitoring a single radical under chemically controlled conditions can offer a greater constraint as to its reaction even with a non-observed parameter.

The issue of parameter control also affects the interpretation of field observations to determine kinetic parameters. Most surprisingly, the determination of k_1 from microwave limb sounder atmospheric measurements reports a value of k_1 in good agreement with laboratory studies, but at a single temperature of T = 245 K. Observations through an atmospheric limb into deep space cannot be probing air at such a fixed, single temperature, with error limits in T of only 1.4 K reported in this study. Such observations are certainly valuable in demonstrating the correlation of ClO and HO_2 loss with generation of HOCl, but a single temperature evaluation of k_1 from such studies appears unrealistic.

Considering the studies of k_1 as a function of temperature, Stimpfle *et al.*[19] measured both HO_2 and ClO concentrations using laser magnetic resonance, at low pressures ($0.8 \leq p/\text{Torr} \leq 3.4$) following their microwave generation in a flow tube. Uniquely, these authors recorded a non-linear temperature dependence for k_1, which they attributed to a more than one form of the $HClO_3$ association complex in the reaction, potentially leading to the different product channels (1a) and (1b). Subsequently, the study of Nickolaisen *et al.*[27] reported a linear negative temperature dependence for k_1, albeit with absolute values for the rate constant close to those reported by Stimpfle *et al.* The other two studies of k_1 carried out as a function of temperature were reported by Knight *et al.*[28] and Hickson *et al.*,[26] both using flow tubes at low pressure. Knight *et al.*[28] used multiple radical sources for the reaction (albeit with ClO always in excess), and reported a near-zero temperature dependence for k_1. By contrast, Hickson *et al.*[26] reported a negative, linear, temperature dependence to k_1, using a variety of radical precursors and experimental arrangements, with the temperature trend (E/R) in k_1 close to that in gradient, although smaller in absolute magnitude of, the results of Nickolaisen *et al.*[27]

The results recorded in the present work were analysed under a number of different scenarios, discussed above, which gave insight into the provenance of the two radicals involved and which gave consequent constraint on the numerical model assumptions of which were tested through sensitivity analysis. The final temperature dependence for k_1 recorded here shows considerable scatter, reflected in the statistical error in the Arrhenius parameters reported. However, the data here exhibit a clear negative temperature dependence in agreement with previous high pressure studies of k_1. As indicated by several previous theoretical studies,[33,42,43] this might imply the collisional stabilisation of a $HClO_3$ moiety at high pressures, in addition to 'bimolecular' channels predominating at low pressures. This may imply, as has also been proposed previously,[42] that the $HClO_3$, specifically HOOOCl, species might form in the lower stratosphere and therefore that the potential photolysis channels of this molecule would govern its atmospheric impact. Only pressure dependent studies of this reaction can confirm or rule this out, which is a future goal. But, at the very least, the data reported in the present study confirm and quantify the efficiency of the HO_2 + ClO reaction and therefore its key role in midlatitude ozone loss.

5. Conclusions

The present study represents a study of the ClO decay chemistry in the presence of HO_2, with a technique (CCD monitoring and multiwavelength/ time resolved spectroscopy) that is especially suited to ClO monitoring. The ClO traces recorded in the absence of methanol, and therefore HO_2 were readily fit to a two reaction model with only small perturbations for physical processes, giving confidence in this monitoring. In the subsequent presence of CH_3OH and excess oxygen, well-established chemistry was used to generate HO_2 and the ClO decay traces exhibited temporal behaviour consistent with a termination reaction of ClO + HO_2. Rate coefficients reported in this work were higher and exhibited a stronger negative temperature dependence than those reported previously, excluding the work of Stimpfle *et al*.,[19] and therefore contradicts the recent work of Kuribayashi *et al.*[30] However, several previous laboratory studies of k_1 were carried out at low pressure, thus the present work is perhaps indicative of a pressure dependent contribution to reaction (1).

6. Tables

Table 1: Kinetic parameters recorded for reversible ClO association in the absence of methanol. Errors are 1σ statistical only. For comparison, calculated values and errors from the recent NASA-JPL recommended expressions[11] are also presented.

T /K	$[ClO]_0$[a] / 10^{14}	k_2[b] / 10^{-13}	k_{-2}[c]	k_2[b] / 10^{-13} NASA-JPL[11]	k_{-2}[c] NASA-JPL[11]
298.15	1.59 – 2.02	(3.89 ± 0.21)	39.98 ± 0.83	(2.68 ± 0.75)	39.2 ± 11.0
278.65	1.70 – 2.18	(5.97 ± 0.09)	6.39 ± 0.37	(3.65 ± 1.02)	7.02 ± 1.99
261.55	2.08 – 2.94	(6.62 ± 0.22)	0.54 ± 0.25	(4.84 ± 1.35)	1.22 ± 0.35
246.45	1.71 – 2.61	(8.63 ± 1.13)	0.16 ± 0.06	(6.26 ± 1.76)	0.21 ± 0.06
232.95	1.63 – 2.20	(10.2 ± 0.23)	0.08 ± 0.15	(7.94 ± 2.23)	0.03 ± 0.01
210.05	1.50 – 2.25	(12.2 ± 0.16)	0.00	(12.1 ± 3.39)	0.00

[a]units of molecules cm^{-3}
[b]units of cm^3 $molecules^{-1}$ s^{-1}
[c]units of s^{-1}

Table 2: Initial ClO radical concentration and rates of change of ClO concentration recorded as a function of methanol vapour concentration at $T = 298$ K.

$[CH_3OH]^a$	$[ClO]_{max}{}^a$	$-\frac{d[ClO]_{no\ CH_3OH}}{dt}{}^b$	$-\frac{d[ClO]}{dt}{}^b$
4.11×10^{15}	1.58×10^{14}	1.67×10^{16}	1.72×10^{16}
5.67×10^{15}	1.30×10^{14}	1.17×10^{16}	1.48×10^{16}
7.23×10^{15}	1.05×10^{14}	7.87×10^{15}	1.30×10^{16}
8.79×10^{15}	8.08×10^{13}	4.78×10^{15}	1.17×10^{16}
7.23×10^{15}	9.44×10^{13}	6.42×10^{15}	1.19×10^{16}
1.03×10^{16}	7.17×10^{13}	3.79×10^{15}	1.13×10^{16}
1.13×10^{16}	6.52×10^{13}	3.16×10^{15}	1.14×10^{16}

[a]units of molecules cm^{-3}
[b]units of cm^3 molecules^{-1} s^{-1}

Table 3: Reaction scheme used for numerical modelling with rate coefficient expressions taken principally from the NASA-JPL data evaluation.[11]

Reaction	Rate constant (T dependent or T = 298 K)
Formation Chemistry	
$Cl + Cl_2O \rightarrow Cl_2 + ClO$	$6.20 \times 10^{-11}\exp(130/T)$
$Cl + CH_3OH \rightarrow CH_2OH + HCl$	5.5×10^{-11}
$CH_2OH + O_2 \rightarrow HCHO + HO_2$	9.1×10^{-11}
Principal Reaction	
$ClO + HO_2 \rightarrow HOCl + O_2$	$2.6 \times 10^{-12}\exp(290/T)$ (Initially)
ClO Competing Chemistry	
$ClO + ClO + M \rightarrow Cl_2O_2 + M$	See Table 1
$Cl_2O_2 + M \rightarrow ClO + ClO + M$	See Table 1
$ClO + ClO \rightarrow Cl_2 + O_2$	$1.00 \times 10^{-12}\exp(-1590/T)$
$ClO + ClO \rightarrow OClO + Cl$	$3.50 \times 10^{-13}\exp(-1370/T)$
$ClO + ClO \rightarrow ClOO + Cl$	$3.00 \times 10^{-11}\exp(-2450/T)$
$Cl + O_2 \rightarrow ClOO$	$k_0 = 2.20 \times 10^{-33} \times (T/300)^{-3.1a}$
$ClOO \rightarrow Cl + O_2$	$k_\infty = 1.80 \times 10^{-10} \times (T/300)^{0}$ $K_{eq} = 6.60 \times 10^{-25}\exp(2502/T)^b$
$ClOO + ClOO \rightarrow ClO + ClO + O_2$	1.60×10^{-11}
$ClOO + Cl_2 \rightarrow Cl_2O + ClO$	3.40×10^{-12}
$ClO + OClO \rightarrow Cl_2O_3$	$k_0 = 1.60 \times 10^{-32} \times (T/300)^{-4.7a}$
$Cl_2O_3 \rightarrow ClO + OClO$	$k_\infty = 3.00 \times 10^{-11} \times (T/300)^{-1.1}$ $K_{eq} = 1.50 \times 10^{-27}\exp(7140/T)^b$
$CH_2OH + Cl_2 \rightarrow Cl + ClCH_2OH$	2.90×10^{-11}
HO_2 Competing Chemistry	
$HO_2 + HO_2 \rightarrow H_2O_2 + O_2$	$1.80 \times 10^{-14}\exp(1500/T)(1 + 0.56 \times 10^{-21} \times [CH_3OH]\exp(2550/T)$ [ref 36]
$HO_2 + Cl \rightarrow HCl + O_2$	$1.40 \times 10^{-11}\exp(270/T)$
$HO_2 + Cl \rightarrow OH + ClO$	$3.60 \times 10^{-11}\exp(-375/T)$
$Cl + H_2O_2 \rightarrow HCl + HO_2$	$1.10 \times 10^{-11}\exp(-980/T)$
Secondary Chemistry	
$HOCH_2O_2 \rightarrow HO_2 + HCHO$	$9.70 \times 10^{-15}\exp(-625/T)$
$HO_2 + HCHO \rightarrow HOCH_2O_2$	$2.40\times10^{12}\exp(7000/T)$
$HOCH_2O_2 + HO_2 \rightarrow HOCH_2OOH + O_2$	$(0.6) \times 5.60\times10^{-15}\exp(-2300/T)$
$HOCH_2O_2 + HO_2 \rightarrow O_2 + HC(O)OH + H_2O$	$(0.4) \times 5.60\times10^{-15}\exp(-2300/T)$
$HOCH_2OOH + Cl \rightarrow HCOOH + OH + HCl$	1.00×10^{-10}
$HOCH_2OOH + Cl \rightarrow HOCH_2O_2 + HCl$	5.00×10^{-10}
$HOCH_2O_2 + HOCH_2O_2 \rightarrow HOCH_2O + HOCH_2O + O_2$	$5.70 \times 10^{-14}\exp(750/T)$
$HOCH_2O_2 + O_2 \rightarrow HCOOH + HO_2$	3.50×10^{-14}
$Cl + HCHO \rightarrow HCl + HCO$	$8.10 \times 10^{-11}\exp(-30/T)$
$HCO + O_2 \rightarrow CO + HO_2$	$3.50 \times 10^{-12}\exp(140/T)$
$HCO + Cl_2 \rightarrow HCOCl + Cl$	$6.10 \times 10^{-12}\exp(-36/T)$

Units of cm^3 $molecules^{-1}$ s^{-1} unless otherwise stated.
[a]units of cm^6 $molecule^{-2}$ s^{-1} and [b]units of cm^3 $molecule^{-1}$

Table 4: Kinetic parameters obtained for reaction (1) along with ranges of initial ClO and added methanol concentrations. The parameter delta represented the partitioning of initial Cl and ClO concentrations (see text for details).

T (K)	$[ClO]_0$[a] / 10^{14}	$[CH_3OH]_0$[a] / 10^{15}	δ	k_1[b] / 10^{-11}
298.15	1.0 – 1.5	7.0 – 10	0.4 – 0.9	0.85 ± 0.15
278.65	1.0 – 1.5	7.2 – 9.7	0.4 – 0.6	1.10 ± 0.40
261.55	1.4 – 1.6	6.7 – 9.7	0.5 – 0.6	1.03 ± 0.17
246.45	1.1 – 1.8	8.7 – 10.1	0.3 – 0.5	0.90 ± 0.08
232.95	1.1 – 1.3	9.2 – 11.1	0.2 – 0.5	1.59 ± 0.21
210.05	1.1 – 1.8	10 – 12.3	0.4 – 0.6	1.70 ± 0.64

[a]units of molecules cm^{-3}
[b]units of cm^3 $molecules^{-1}$ s^{-1}

7. Figures

Figure 1: Histogram of previous determinations of k_1 at T = 298 K, with associated errors. Red bars refer to low pressure (p < 10 Torr) studies, typically from flow tubes. Blue bars refer to high pressure (p > 50 Torr) studies, typically from static or flash photolysis experiments. Violet bars indicate the current recommendations for k_1 from JPL-NASA[11] and IUPAC[25] data evaluations.

Figure 2: Arrhenius plot for determinations of k_1. Red squares = Stimpfle *et al.*, green triangles = Hickson *et al.*, blue diamonds = Nickolaisen *et al.*, Blue triangles = Knight *et al.*, black circles = this work.

Figure 3: Time-averaged post photolysis spectra recorded under methanol free conditions (black), and in the presence of $[CH_3OH] = 1.1 \times 10^{16}$ molecules cm^{-3}.

Figure 4a: Three separate kinetic experiments showing $[ClO]_t$ traces before addition of CH_3OH to the system (green), with CH_3OH in the system (blue) and after removal of CH_3OH from the system (black). The kinetic fits to the temporal data are shown by the red line (in the absence of methanol) and the blue line (in the presence of methanol), invoking k_1.

Figure 4b: A single $[ClO]_t$ trace (black) recorded in the presence of methanol, $[CH_3OH] = 1.1 \times 10^{16}$ molecules cm^{-3} with a simulated trace incorporating the ClO + HO_2 chemistry (red) and ClO dimerization only kinetics (green). Offset residuals × 5 for the ClO + HO_2 reaction fit are shown in blue.

Figure 5: [ClO] temporal traces showing the effect of added methanol (values as given in Table 2), showing the progressive reduction of $[ClO]_0$ with increased $[CH_3OH]$ but an increased rate of ClO loss at lower $[ClO]_0$.

Figure 6: The variation of the initial rate of $[ClO]_t$ decay as a function of $[ClO]_0$ as observed in the presence of methanol (black) and modelled rates on the basis of a ClO dimerization only scheme.

Figure 7: Maximum $[ClO]_0$ as a function of added $[CH_3OH]$.

Figure 1

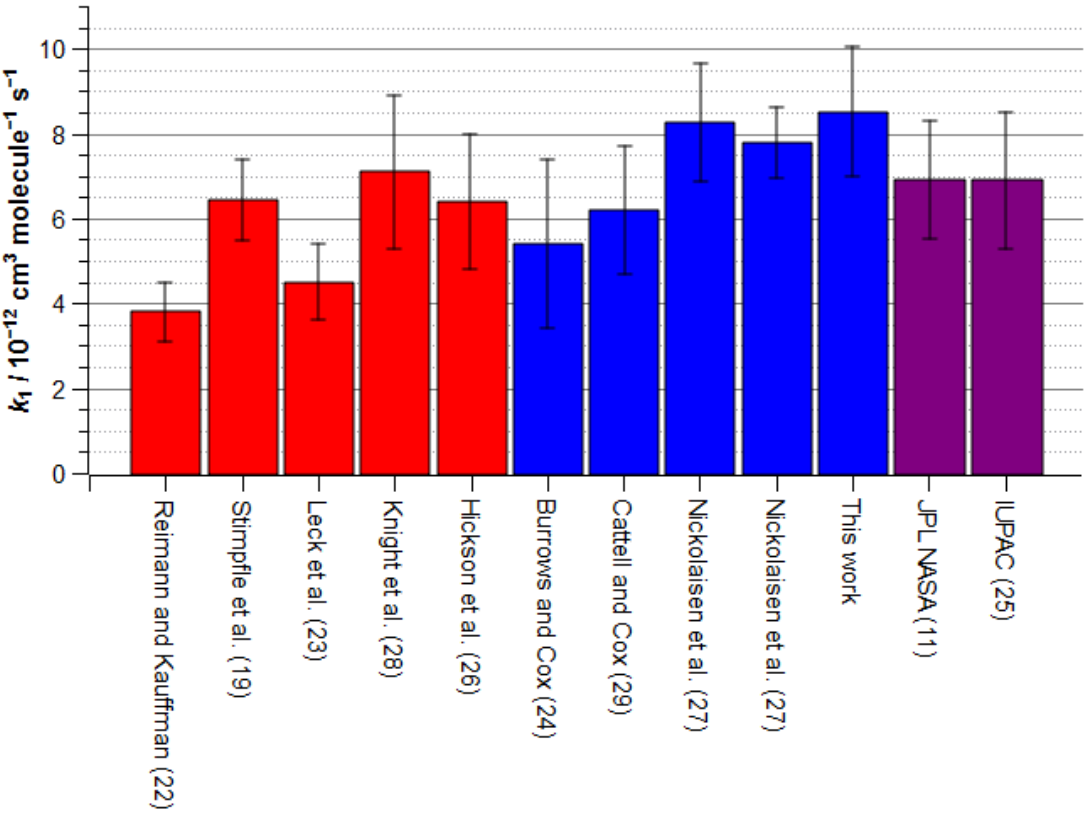
k_1 / 10^{-12} cm^3 molecule^{-1} s^{-1}
0
2
4
6
8
10
Reimann and Kauffman (22)
Stimpfle et al. (19)
Leck et al. (23)
Knight et al. (28)
Hickson et al. (26)
Burrows and Cox (24)
Cattell and Cox (29)
Nickolaisen et al. (27)
Nickolaisen et al. (27)
This work
JPL NASA (11)
IUPAC (25)

Figure 2

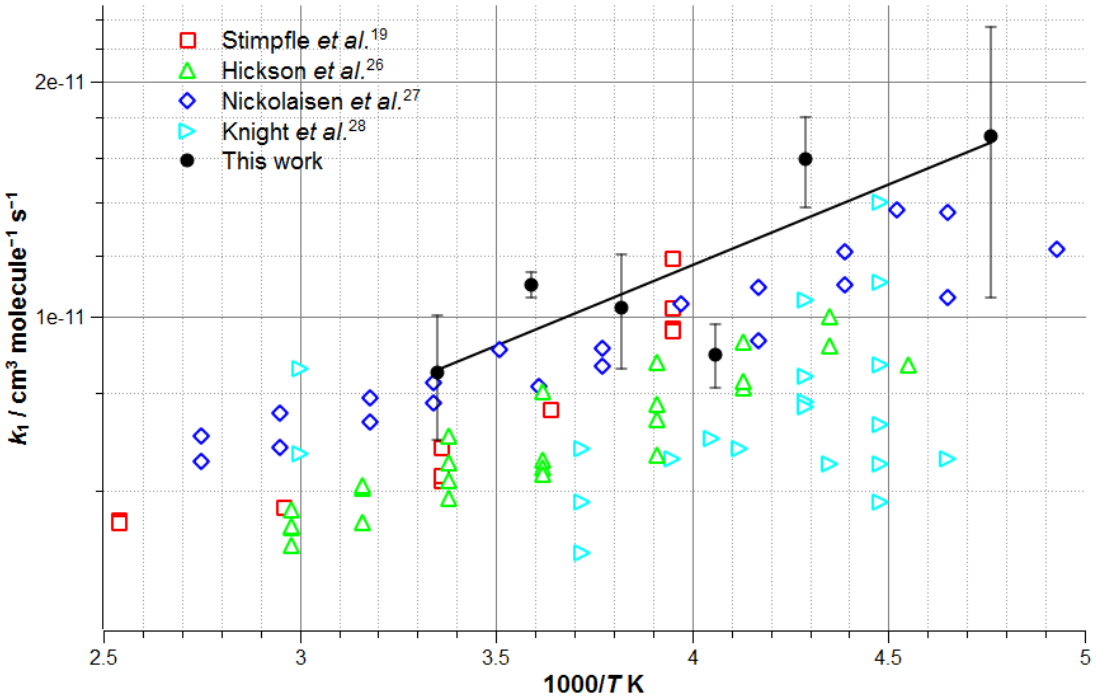
Stimpfle et al.[19]
Hickson et al.[26]
Nickolaisen et al.[27]
Knight et al.[28]
This work
2e-11
1e-11
k1 / cm3 molecule-1 s-1
2.5
3
3.5
4
4.5
5
1000/T K

Figure 3

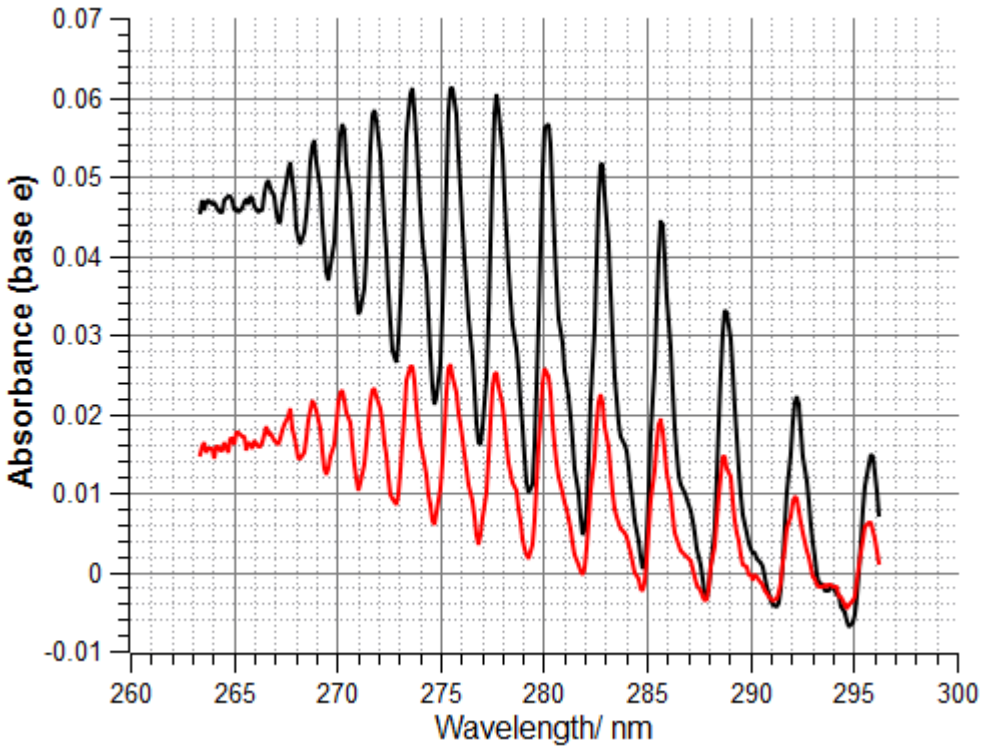
Absorbance (base e)
0.07
0.06
0.05
0.04
0.03
0.02
0.01
0
-0.01
260
265
270
275
280
285
290
295
300
Wavelength/ nm

Figure 4a

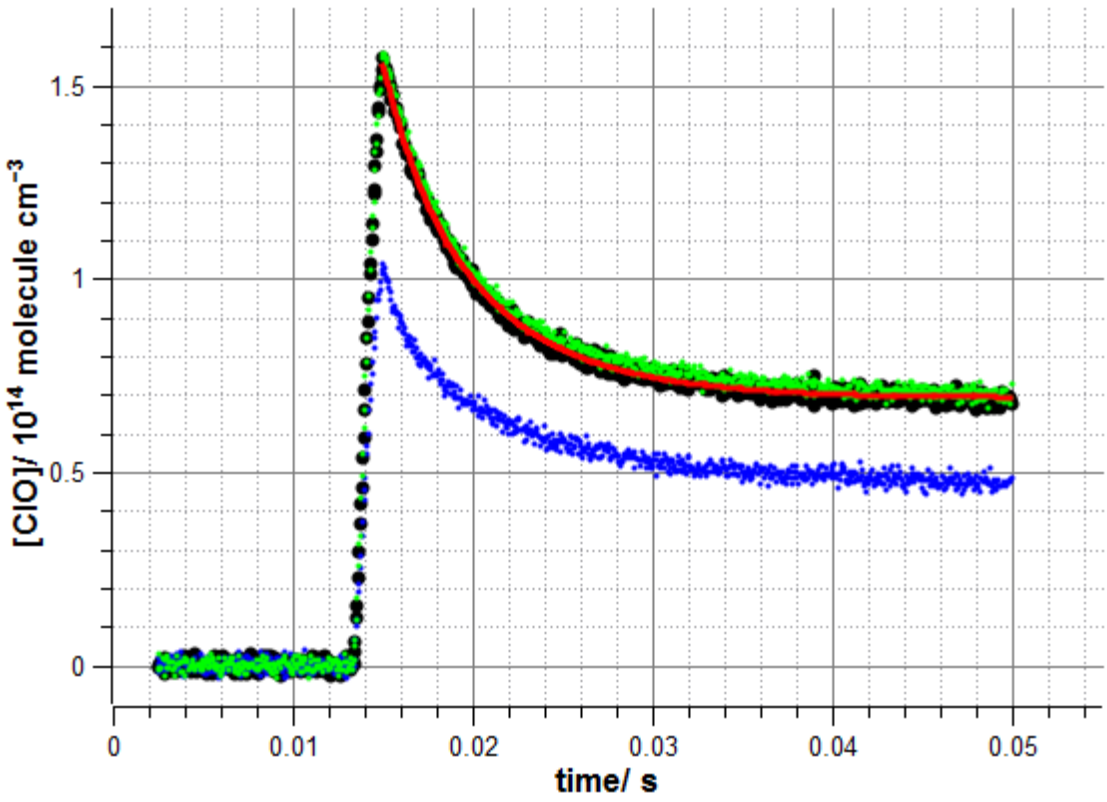

Figure 4b

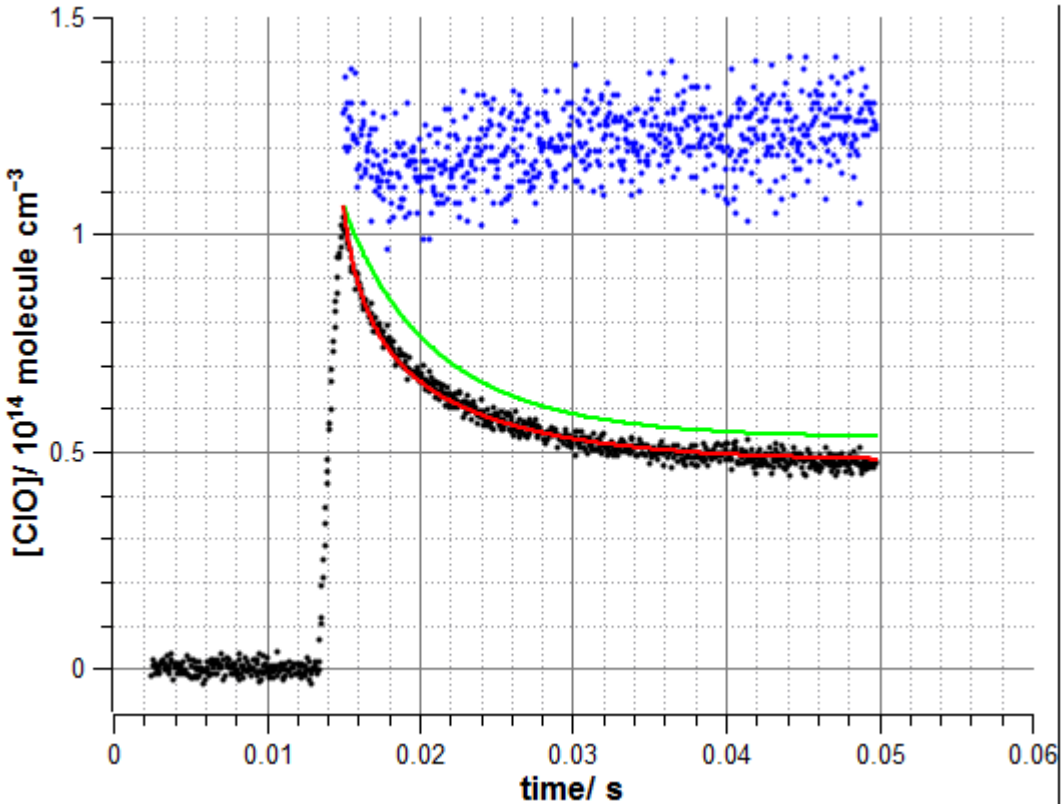

Figure 5

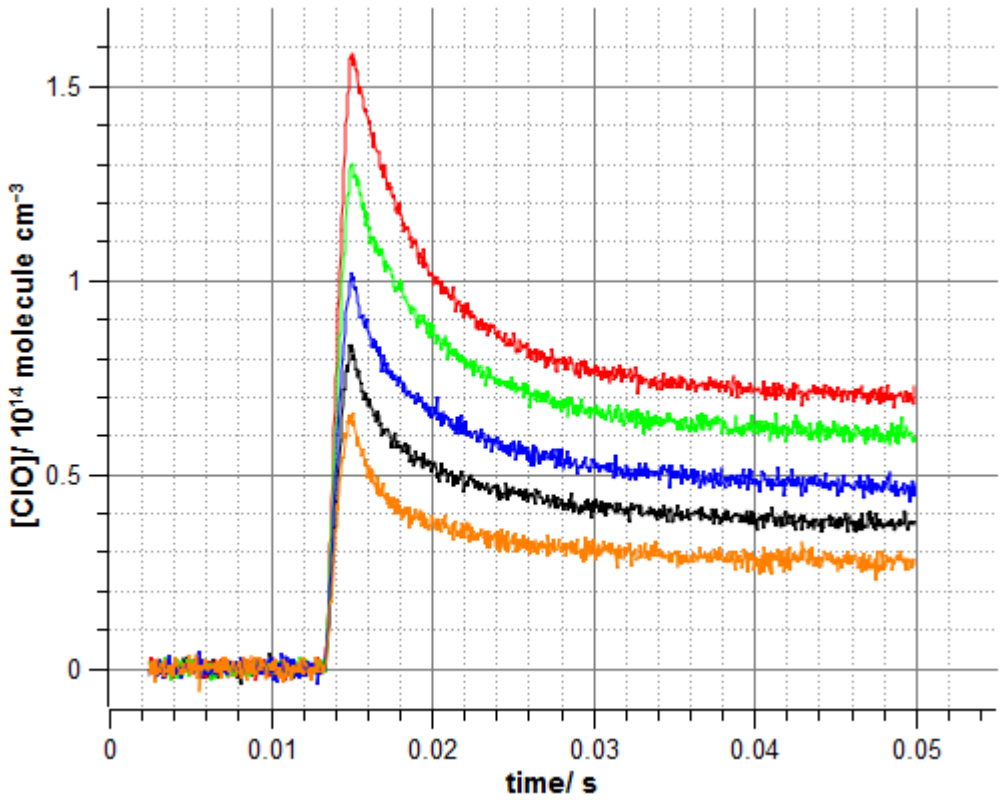

Figure 6

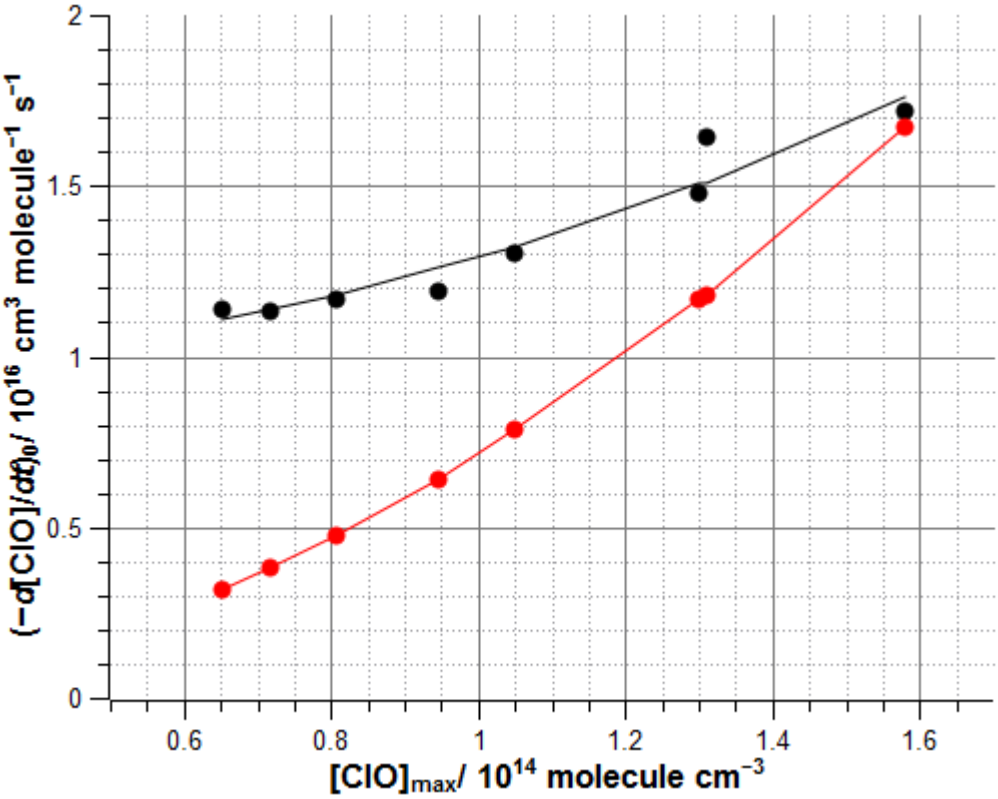
2
1.5
1
0.5
0
0.6
0.8
1
1.2
1.4
1.6
$(-d[ClO]/dt)_0$/ 10^{16} cm^3 molecule^{-1} s^{-1}
$[ClO]_{max}$/ 10^{14} molecule cm^{-3}

Figure 7

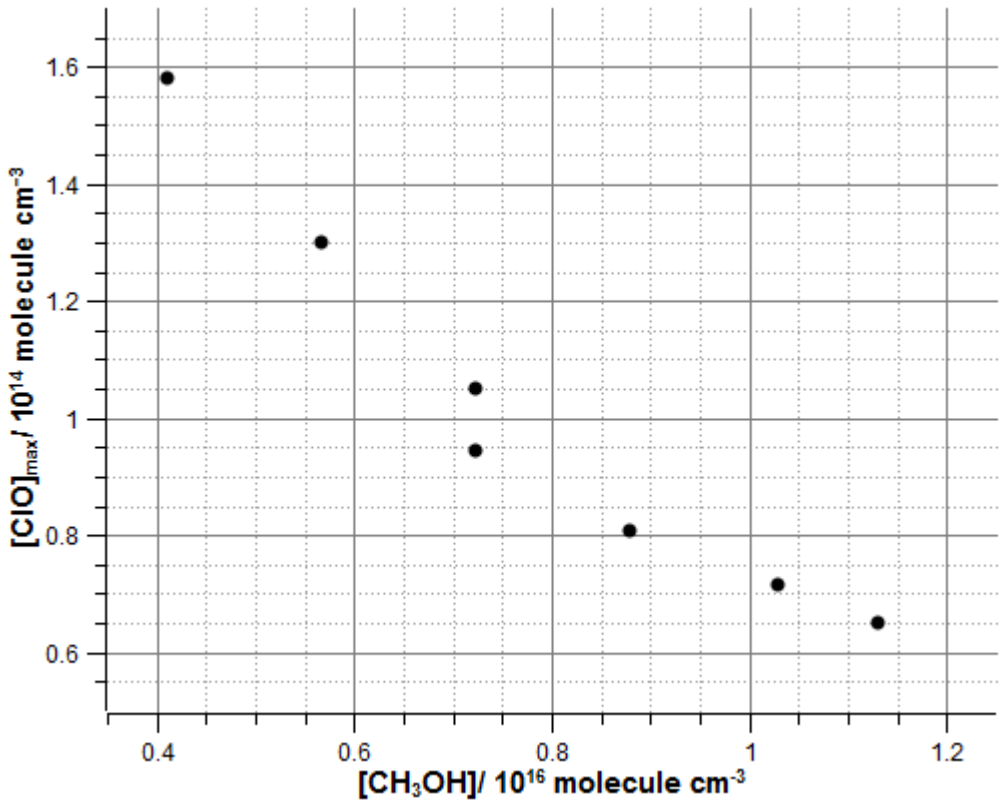
1.6
1.4
1.2
1
0.8
0.6
0.4
0.6
0.8
1
1.2
[ClO]max/ 10^14 molecule cm^-3
[CH3OH]/ 10^16 molecule cm^-3

8. References

1. WMO, *(World Meteorological Organization), Scientific Assessment of Ozone Depletion: 2010, Global Ozone Research and Monitoring Project-Report No. 52, 516 pp., Geneva, Switzerland,* 2011
2. Farman, J.C., B.G. Gardiner, and J.D. Shanklin, *Nature*, 1985, **315**, 207-210.
3. Manney, G.L., M.L. Santee, M. Rex, N.J. Livesey, M.C. Pitts, P. Veefkind, E.R. Nash, I. Wohltmann, R. Lehmann, L. Froidevaux, L.R. Poole, M.R. Schoeberl, D.P. Haffner, J. Davies, V. Dorokhov, H. Gernandt, B. Johnson, R. Kivi, E. Kyro, N. Larsen, P.F. Levelt, A. Makshtas, C.T. McElroy, H. Nakajima, M.C. Parrondo, D.W. Tarasick, P. von der Gathen, K.A. Walker, and N.S. Zinoviev, *Nature*, 2011, **478**, 429-434.
4. Santee, M.L., G.L. Manney, N.J. Livesey, L. Froidevaux, M.J. Schwartz, and W.G. Read, *J. Geophys. Res. Atmos.*, 2011, **116**, D18306.
5. Rowland, F.S., *Phil. Trans. Roy. Soc. B-Bio. Sci.*, 2006, **361** 769-790.
6. Molina, L.T. and M.J. Molina, *J. Phys. Chem.*, 1987, **91**, 433-436.
7. Anderson, J.G., D.W. Toohey, and W.H. Brune, *Science*, 1991, **251**, 39-46.
8. Solomon, S., R.R. Garcia, F.S. Rowland, and D.J. Wuebbles, *Nature*, 1986, **321**, 755-758.
9. Borrmann, S., S. Solomon, J.E. Dye, and B.P. Luo, *Geophys. Res. Let.*, 1996. **23**, 2133-2136.
10. Meier, R.R., G.P. Anderson, C.A. Cantrell, L.A. Hall, J. Lean, K. Minschwaner, R.E. Shetter, E.P. Shettle, and K. Stamnes, *J. Atmos. Solar-Terrestrial Phys.*, 1997, **59**, 2111-2157.
11. Sander, S.P., J. Abbatt, J. R. Barker, J. B. Burkholder, R. R. Friedl, D. M. Golden, R. E. Huie, C. E. Kolb, M. J. Kurylo, G. and V.L.O. K. Moortgat, P. H. Wine, "Chemical Kinetics and Photochemical Data for Use in Atmospheric Studies, Evaluation No. 17," JPL Publication 10-6, Jet Propulsion Laboratory, Pasadena, 2011 http://jpldataeval.jpl.nasa.gov.
12. Gettelman, A., P. Hoor, L.L. Pan, W.J. Randel, M.I. Hegglin, and T. Birner, *Rev. Geophys.*, 2011, **49,** RG3003.
13. Johnson, D.G., W.A. Traub, K.V. Chance, K.W. Jucks, and R.A. Stachnik, *Geophys. Res. Let.*, 1995, **22**, 1869-1871.
14. Danielsen, E.F., *Geophys. Res. Let.*, 1982, **9**, 605-608.
15. Khaykin, S., J.P. Pommereau, L. Korshunov, V. Yushkov, J. Nielsen, N. Larsen, T. Christensen, A. Garnier, A. Lukyanov, and E. Williams, *Atmos. Chem. Phys.*, 2009, **9**, 2275-2287.
16. Pommereau, J.P., *Comptes Rendus Geoscience*, 2010, **342**, 331-338.

17. Kovalenko, L.J., K.W. Jucks, R.J. Salawitch, G.C. Toon, J.F. Blavier, D.G. Johnson, A. Kleinbohl, N.J. Livesey, J.J. Margitan, H.M. Pickett, M.L. Santee, B. Sen, R.A. Stachnik, and J.W. Waters, *Geophys. Res. Let.*, 2007, **34**, L19801.
18. von Clarmann, T., B. Funke, N. Glatthor, S. Kellmann, M. Kiefer, O. Kirner, B.M. Sinnhuber, and G.P. Stiller, *Atmos. Chem. Phys.*, 2012, **12**, 1965-1977.
19. Stimpfle, R.M., R.A. Perry, and C.J. Howard, *J. Chem. Phys.*, 1979, **71**, 5183-5190.
20. Anderson, J.G., D.M. Wilmouth, J.B. Smith, and D.S. Sayres, *Science*, 2012. **337**, 835-839.
21. von Hobe, M., J.U. Grooss, G. Gunther, P. Konopka, I. Gensch, M. Kramer, N. Spelten, A. Afchine, C. Schiller, A. Ulanovsky, N. Sitnikov, G. Shur, V. Yushkov, F. Ravegnani, F. Cairo, A. Roiger, C. Voigt, H. Schlager, R. Weigel, W. Frey, S. Borrmann, R. Muller, and F. Stroh, *Atmos. Chem. Phys.*, 2011, **11**, 241-256.
22. Reimann, B. and F. Kaufman, *J. Chem. Phys.*, 1978, **69**, 2925-2926.
23. Leck, T.J., J.E.L. Cook, and J.W. Birks,. *J. Chem. Phys.*, 1980, **72**, 2364-2373.
24. Burrows, J.P. and R.A. Cox, *J. Chem. Soc.-Far. Trans. I*, 1981, **77**, 2465-2479.
25. Atkinson, R., D.L. Baulch, R.A. Cox, J.N. Crowley, R.F. Hampson, R.G. Hynes, M.E. Jenkin, M.J. Rossi, and J. Troe, *Atmos. Chem. Phys.*, 2007. **7**: 981-1191.
26. Hickson, K.M., L.F. Keyser, and S.P. Sander, *J. Phys. Chem. A*, 2007, **111**, 8126-8138.
27. Nickolaisen, S.L., C.M. Roehl, L.K. Blakeley, R.R. Friedl, J.S. Francisco, R.F. Liu, and S.P. Sander, *J. Phys. Chem. A*, 2000, **104**, 308-319.
28. Knight, G.P., T. Beiderhase, F. Helleis, G.K. Moortgat, and J.N. Crowley, *J. Phys. Chem. A*, 2000, **104**, 1674-1685.
29. Cattell, F.C. and R.A. Cox, *J. Chem. Soc.-Far. Trans. II*, 1986, **82**, 1413-1426.
30. Kuribayashi, K., H. Sagawa, R. Lehmann, T.O. Sato, and Y. Kasai, *Atmos. Chem. Phys.*, 2014, **14**, 255-266.
31. Finkbeiner, M., J.N. Crowley, O. Horie, R. Muller, and G.K. Moortgat, *J. Phys. Chem.*, 1995, **99**, 16264-16275.
32. Leu, M.T., *Geophys. Res. Let.*, 1980, **7,** 173-175.
33. Zhu, R.S. and M.C. Lin, *Comp. and Theor. Chem.*, 2011, **965**, 328-339.
34. Ferracci, V. and D.M. Rowley, *Phys. Chem. Chem. Phys.*, 2010, **12**, 11596-11608.
35. Rowley, D.M., M.H. Harwood, R.A. Freshwater, and R.L. Jones, *J. Phys. Chem.*, 1996. **100**, 3020-3029.
36. Stone, D. and D.M. Rowley, *Phys. Chem. Chem. Phys.*, 2005, **7**, 2156-2163.
37. Hinshelwood, C.N. and C.R. Prichard, *J. Chem. Soc.*, 1923, **123**, 2730-2738.

38. Boakes, G., W.H.H. Mok, and D.M. Rowley, *Phys. Chem. Chem. Phys.*, 2005, **7**,4102-4113.
39. Bloss, W.J., D.M. Rowley, R.A. Cox, and R.L. Jones, *Phys. Chem. Chem. Phys.*, 2002, **4**, 3639-3647.
40. Christensen, L.E., M. Okumura, J.C. Hansen, and S.P. Sander, *J. Phys. Chem. A*, 2006, **110,** 6948-6959.
41. Tang, Y.X., G.S. Tyndall, and J.J. Orlando, *J. Phys. Chem. A*, 2010, **114**, 369-378.
42. Kaltsoyannis, N. and D.M. Rowley, *Phys. Chem. Chem. Phys.*, 2002, **4**, 419-427.
43. Xu, Z.F., R.S. Zhu, and M.C. Lin, *J. Phys. Chem. A*, 2003, **107**, 3841-3850.